ACS APPLIED MATERIALS & INTERFACES

Research Article

www.acsami.org

Hydrogen Silsequioxane-Derived Si/SiO_x Nanospheres for High-Capacity Lithium Storage Materials

Min-Sik Park,[†,∥] Eunjun Park,[‡,∥] Jaewoo Lee,[†] Goojin Jeong,[†] Ki Jae Kim,[†] Jung Ho Kim,[§,⊥] Young-Jun Kim,*[,†] and Hansu Kim*[,‡]

[†]Advanced Batteries Research Center, Korea Electronic Technology Institute, 68 Yatap-dong, Bundang-gu, Seongnam 463-816, Republic of Korea

[‡]Department of Energy Engineering, Hanyang University, 222 Wangsimni-ro, Seongdong-gu, Seoul 133-791, Republic of Korea

[§]Institute for Superconducting and Electronic Materials, University of Wollongong, North Wollongong, New South Wales 2500, Australia

[⊥]Department of Physics and Astronomy, College of Science, P.O. Box 2455, King Saud University, Riyadh 11451, Kingdom of Saudi Arabia

Supporting Information

ABSTRACT: Si/SiO_x composite materials have been explored for their commercial possibility as high-performance anode materials for lithium ion batteries, but suffer from the complexity of and limited synthetic routes for their preparation. In this study, Si/SiO_x nanospheres were developed using a nontoxic and precious-metal-free preparation method based on hydrogen silsesquioxane obtained from sol–gel reaction of triethoxysilane. The resulting Si/SiO_x nanospheres with a uniform carbon coating layer show excellent cycle performance and rate capability with high-dimensional stability. This approach based on a scalable sol–gel reaction enables not only the development of Si/SiO_x with various nanostructured forms, but also reduced production cost for mass production of nanostructured Si/SiO_x.

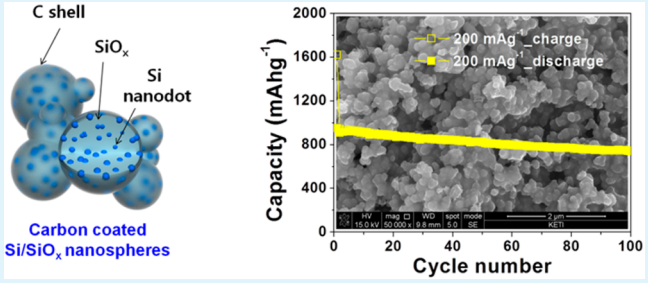

KEYWORDS: *anode, hydrogen silsesquioxane, lithium ion batteries, nanoparticles, silicon, silicon oxides*

INTRODUCTION

With the growing market for electric vehicles, lithium ion batteries (LIBs) have received a great deal of attention as suitable power sources owing to their high energy and power densities. Over the past several decades, the main challenge facing LIBs has been finding new materials which can deliver higher capacities than currently commercialized materials.[1−3] Silicon (Si) has been regarded as a promising anode material for LIBs because of its highest theoretical capacity (~3580 mA h g^{-1}, $Li_{15}Si_4$) among alloy-type anode materials and relatively low discharge potential (~0.4 V vs Li/Li^+).[4] Despite its attractive features, the practical use of Si is still limited by its poor cycle performance, which is associated with its severe volume changes during Li^+ insertion and extraction.[4−9] In an attempt to overcome these limitations of Si, much attention has been devoted to the nanoengineering of Si. A technical breakthrough has been made by confining active Si on the nanoscale, which is advantageous to effectively minimize the mechanical strains induced by the volume changes of Si.[10−17]

In particular, the Si/SiO_x composite, in which crystalline Si is confined in an amorphous SiO_x matrix, showed drastically improved anode performance compared to Si.[18,19] The amorphous SiO_x matrix allows for effective accommodation of the volume changes of the confined crystalline Si undergoing a partially reversible reaction with Li^+, resulting in a high reversible capacity and good cycle performance. Nevertheless, Si/SiO_x composites still have some drawbacks that need to be resolved before wide usage in LIBs is possible, especially because their cost is much higher than that of graphite. Until now, most Si/SiO_x composites, including SiO, have been obtained by an expensive fabrication process involving vacuum evaporation of Si and SiO_2 at high temperatures (above 1400 °C).[20,21] One can reasonably expect that nanostructured Si/SiO_x composites would be more favorable for electrochemical reactions with Li^+. Recently, Yoo et al. reported a Si/SiO_x urchinlike structure obtained by chemical etching of Pt-decorated Si with HF.[19] Chemical etching of Si may be a more promising process than vacuum evaporation, as chemical etching of Si particles may not only reduce the production cost, but also enable various Si/SiO_x nanostructures. The issues related to the use of toxic chemicals (HF) and precious metals (Pt) need to be further addressed, however, on the basis of

Received: April 3, 2014
Accepted: May 20, 2014
Published: May 20, 2014

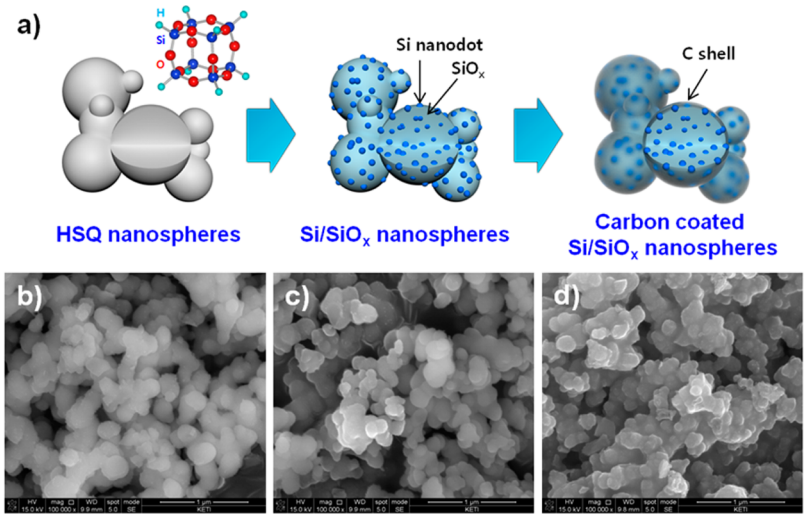

Figure 1. (a) Schematic illustration of the proposed synthetic route for C-coated Si/SiO_x nanospheres. FESEM images of (b) HSQ nanospheres prepared by a sol–gel reaction of triethoxysilane, (c) HSQ-derived Si/SiO_x nanospheres obtained by the heat treatment of HSQ nanospheres at 1200 °C under an Ar-balanced 4% H_2 atmosphere, and (d) C-coated Si/SiO_x nanospheres after the pyrolysis of pitch at 1000 °C under a N_2 atmosphere.

production costs and safety. Our major concern for the development of Si/SiO_x composites is to find a scalable synthetic route combined with proper nanostructures, as current synthetic methods are highly limited for mass production, as well as for rationally designed Si/SiO_x nanostructures.

Herein, we demonstrate a highly efficient but scalable synthetic route based on hydrogen silsesquioxane ($HSiO_{1.5}$, HSQ) to produce a nanostructured Si/SiO_x composite as a high-capacity lithium storage material. Using a sol–gel reaction of triethoxysilane in an aqueous medium,[22−25] we synthesized Si/SiO_x nanospheres with a size of 100–200 nm, in which crystalline Si nanodots about 5 nm in size are integrated into the amorphous SiO_x matrix. We formed a uniform carbon shell on the surface of the Si/SiO_x nanospheres to improve electrical conductivity. The resulting C-coated Si/SiO_x nanospheres exhibited a high reversible capacity and outstanding cycle performance. Besides its ability to simplify the production process, it is worth emphasizing that our sol–gel approach has the capacity to produce various forms of Si/SiO_x nanostructures which could not prepared using conventional synthetic routes.

EXPERIMENTAL SECTION

Material Preparation. To prepare the HSQ–Si/SiO_x nanospheres, 5 mL of triethoxysilane ($(C_2H_5O)_3SiH$; Aldrich, 99.8%) was first slowly dropped into a 0.1 M HCl solution (250 mL) under continuous stirring at 800 rpm. The solution was filtered and washed with deionized water repeatedly. The precipitates were collected and dried in a vacuum oven at 110 °C to eliminate residual moisture. After fine grinding, the obtained powder was heated at 1200 °C under a 4% H_2/Ar atmosphere with a flow rate of 0.5 L min^{-1}. The heating rate and time were fixed at 20 °C min^{-1} and 1 h, respectively. For a uniform C coating, the obtained Si/SiO_x nanospheres were thoroughly mixed with coal-tar pitch in a weight ratio of 7:3. The mixture was loaded into a vertical furnace and heated at 1000 °C for 2 h under a N_2 atmosphere. The final spherical C-coated Si/SiO_x nanospheres were collected and physically ground before use.

Structural Characterizations. The morphologies and microstructures of the Si/SiO_x nanospheres and C-coated Si/SiO_x nanospheres were examined using field emission scanning electron microscopy (FESEM; JEOL JSM-7000F) and high-resolution transmission electron microscopy (HRTEM; JEOL 2100F). Powder X-ray diffraction (XRD) patterns of the Si/SiO_x and C-coated Si/SiO_x nanospheres were obtained using an X-ray diffractometer (Empyrean, PANanalytical) equipped with a 3D pixel semiconductor detector using Cu Kα radiation (λ = 1.54056 Å). Raman and FT-IR spectra of the Si/SiO_x and C-coated Si/SiO_x nanospheres were collected using a Raman spectrometer (Bruker Senterra Grating 400) with a He–Ne laser at a wavelength of 532 nm and a Fourier transform infrared (FT-IR) spectrophotometer (Bruker VERTEX70), respectively. For further characterization of the surface chemistry of the Si/SiO_x nanospheres, X-ray photoelectron spectroscopy (XPS; Thermo Scientific Sigma Probe) was employed. ^{29}Si magic angle spinning nuclear magnetic resonance (MAS NMR; Bruker ADVANCE 400 WB) was conducted to determine the chemical environment of Si in the Si/SiO_x nanospheres. The samples were spun at 5 kHz, and the number of scans used was 500. The amount of C in the C-coated Si/SiO_x nanospheres was confirmed by thermogravimetric analysis (TGA; PerkinElmer TG/DTA 6300).

Electrochemical Measurements. The electrodes were prepared by coating slurries containing the C-coated Si/SiO_x nanospheres (80 wt %) as active materials, conducting agent (Super-P, 10 wt %), and polyacrylic acid binder (PAA, 10 wt %) dissolved in deionized water on Cu foil. After coating, the electrode was dried at 120 °C for 10 h and pressed under a pressure of 200 kg cm^{-2}. For comparative purposes, the loading amount and density of the electrodes were fixed at 1.5 mg cm^{-2} and 1.0 g cm^{-3}, respectively. The CR2032 coin type half-cells were carefully assembled in an Ar-filled glove box to evaluate their electrochemical performance. A porous polyethylene (PE) membrane was used as a separator, and the electrolyte was 1 M $LiPF_6$ dissolved in a mixed solvent of ethylene carbonate (EC) and dimethyl carbonate (DMC) (3:7, v/v; Panax Etec Co. Ltd.). The cells were galvanostatically charged (Li^+ insertion) and discharged (Li^+ extraction) in the voltage range of 0.01–2.0 V vs Li/Li^+ at different current densities at room temperature.

RESULTS AND DISCUSSION

Figure 1a contains a schematic illustration of the proposed synthetic route for C-coated Si/SiO_x nanospheres in this work. HSQ nanospheres were prepared by a sol–gel reaction of triethoxysilane (Figure 1b). After heat treatment at 1200 °C under a H_2 atmosphere, HSQ-derived Si/SiO_x nanospheres were successfully obtained (Figure 1c). The Si/SiO_x nanospheres retained the particle shape and size of the precursor,

dx.doi.org/10.1021/am5019429 | ACS Appl. Mater. Interfaces 2014, 6, 9608–9613

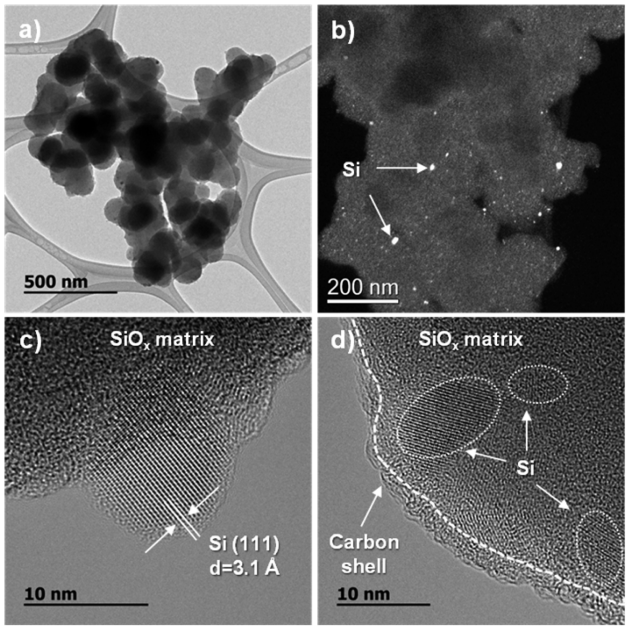

Figure 2. (a) Bright-field TEM image and (b) dark-field TEM image of HSQ-derived Si/SiO_x nanospheres prepared by the sol–gel method. (c) HRTEM image of a crystalline Si nanodot embedded in a SiO_x matrix in the HSQ-derived Si/SiO_x nanospheres. (d) HRTEM image of C-coated Si/SiO_x nanospheres.

which was about 100–200 nm, except that the Si/SiO_x nanospheres became sintered together, resulting in a dumbbell shape. Finally, amorphous C was coated on the surface of the Si/SiO_x nanospheres by pyrolysis of coal-tar pitch under optimized conditions (Figure 1d).

Figure 2a shows that the heat treatment caused the Si/SiO_x nanospheres to be formed into porous secondary particles with a large surface area of 19.7 m^2 g^{-1} (Figure S1, Supporting Information). The dark-field transmission electron microscopy (TEM) image (Figure 2b) shows abundant crystalline Si nanodots (white) embedded in the SiO_x matrix (gray). A closer observation (Figure 2c) confirmed that the crystalline Si nanodots originated from the thermal decomposition of HSQ at 1200 °C.[22−25] The *d* spacing of the confined crystalline Si nanodots was about 3.1 Å, corresponding to crystalline Si(111). An HRTEM image of the C-coated Si/SiO_x nanospheres clearly shows Si nanodots smaller than 10 nm confined in the amorphous matrix (Figure 2d) and an amorphous C layer with a thickness of less than 5 nm on the surface of the Si/SiO_x nanospheres.

Various analytical techniques were employed to study the microstructure of the Si/SiO_x nanospheres in more detail. From the XRD pattern of the Si/SiO_x nanospheres (Figure S2, Supporting Information), we found a broad peak at 2θ = 21.8°, which is a general characteristic of amorphous silicon suboxides, together with the Bragg peak of crystalline Si (2θ = 28.6°), which confirms that the crystalline Si nanodots are well confined in the amorphous SiO_x matrix. The Raman spectrum of a Si/SiO_x nanosphere (Figure 3a) shows a single Raman band at 519.6 cm^{-1}, which is slightly shifted compared to that of the Si reference (519.3 cm^{-1}).[26] This shift can be attributed to the strong optical phonon mode of Si nanodots confined in the SiO_x matrix.[27] The FT-IR spectrum of the Si/SiO_x nanospheres shows small bands at 1122, 809, and 476 cm^{-1} (Figure 3b), indicating that the FT-IR bands correspond to the

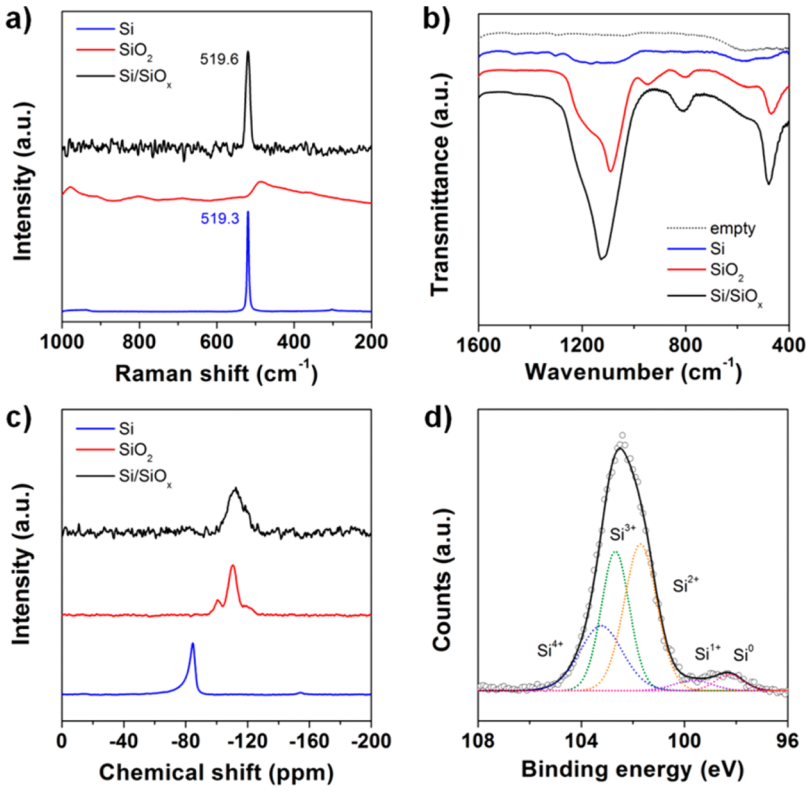

Figure 3. Comparisons of (a) Raman spectra , (b) FT-IR spectra, (c) ^{29}Si MAS NMR spectra, and (d) XPS Si 2p signals collected from HSQ-derived Si/SiO_x nanospheres with those of the Si and SiO_2 references shown for comparison.

dx.doi.org/10.1021/am5019429 | ACS Appl. Mater. Interfaces 2014, 6, 9608–9613

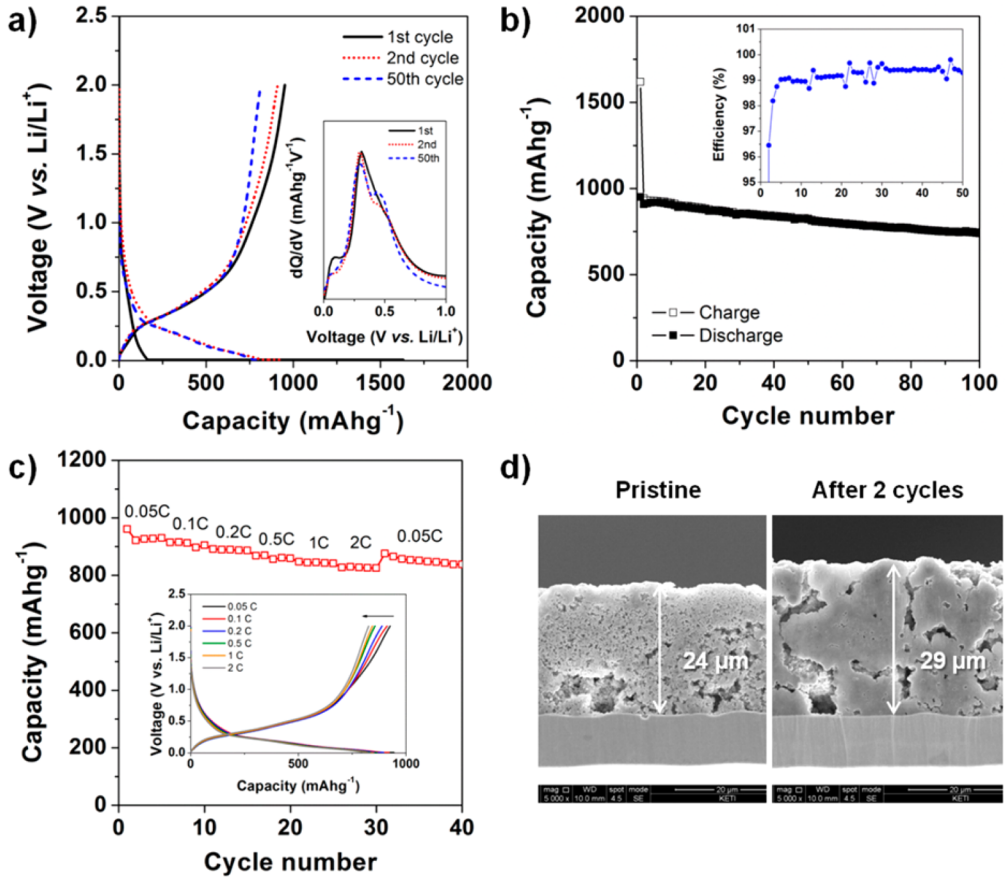

Figure 4. Electrochemical measurements on C-coated Si/SiO_x nanospheres: (a) galvanostatic charge and discharge profiles in the voltage range of 0.01−2.0 V vs Li/Li^+ at a constant current of 0.2 C (200 mA g^{-1}) for the 1st, 2nd, and 50th cycles, together with the corresponding dQ/dV profiles (inset), (b) cycle performance and Coulombic efficiencies (inset) of C-coated Si/SiO_x electrodes at a constant current of 0.2 C (200 mA g^{-1}) for 100 cycles, (c) rate capability of a C-coated Si/SiO_x electrode at different currents of 0.05, 0.1, 0.2, 0.5, 1.0, and 2.0 C (1 C = 1000 mA g^{-1}) in the given voltage range, (d) cross-sectional FESEM images of C-coated Si/SiO_x electrodes [pristine electrode (left) and cycled electrode after two cycles (right)].

Si−O bond and were shifted in the Si/SiO_x nanospheres owing to the nonstoichiometric SiO_x structure.[28] This demonstrates that nonstoichiometric silicon suboxides preferentially form under our synthetic conditions instead of stoichiometric silicon oxides, either SiO or SiO_2.

To further clarify the chemical environment of Si in the Si/SiO_x nanospheres, we carried out ^{29}Si MAS NMR analysis. As shown in Figure 3c, ^{29}Si chemical shifts were observed in the range between −60 and −160 ppm. The Si reference has a strong chemical shift at −83 ppm, which corresponds to Si atoms covalently bonded with neighboring Si atoms,[29] while the SiO_2 reference shows a dominant chemical shift at −110 ppm arising from tetravalent Si (4+).[30] Interestingly, the Si/SiO_x nanospheres show a dominant chemical shift at −109 ppm and a small and broad chemical shift at −81 ppm. Since the chemical shift of Si shows a linear relationship with the oxidation state of Si, the Si/SiO_x nanospheres may be mainly composed of amorphous silicon suboxides with a small amount of crystalline Si nanodots. Figure 3d shows the Si 2p XPS signal obtained from the Si/SiO_x nanospheres after correction of the charging based on C 1s excitation at 284.5 eV. Two dominant peaks were observed at 101.7 and 102.7 eV, which correspond to Si^{3+} and are a general feature of nonstoichiometric silicon suboxides, while the peaks related to Si^{4+} (103.2 eV) and elemental Si (99.6 and 98.2 eV) showed relatively small intensities.[30] From these results, we concluded that HSQ-derived Si/SiO_x nanospheres are composed of Si nanodots and a nonstoichiometric silicon suboxide amorphous matrix. Note that the amount of C was measured to be about 22.9 wt %, on the basis of the TGA results, and SiC was not formed during the carbonization of the pitch (Figure S3 and S4, Supporting Information).

Figure 4a shows the voltage profiles of a C-coated Si/SiO_x electrode at a current density of 0.2 C (200 mA g^{-1}) for the 1st, 2nd, and 50th cycles. The electrode exhibited an initial discharge (Li^+ extraction) capacity of 951.4 mA h g^{-1} with an initial Coulombic efficiency of 58.4%. The corresponding dQ/dV profiles (inset of Figure 4a) show a main peak at around 0.4 V vs Li/Li^+, corresponding to electrochemical reactions between Si and Li^+,[31] which implies that crystalline Si (Si nanodots) is mainly responsible for the reversible Li^+ insertion and extraction. Figure 4b shows the excellent cycle performance of the C-coated Si/SiO_x electrode over 100 cycles without significant capacity fading. The C-coated Si/SiO_x electrode maintained 78% of its initial discharge capacity (740 mA h g^{-1}), even after 100 cycles. More interestingly, the C-coated Si/SiO_x electrodes showed superior Coulombic efficiencies during cycling (inset of Figure 4b). The efficiencies reached more than 99.5% and were maintained even up to 100 cycles. Given that the Coulombic efficiency of the electrode is the critical factor for cycle performance of the full cell, the high Coulombic efficiencies of C-coated Si/SiO_x electrodes represent a key

dx.doi.org/10.1021/am5019429 | ACS Appl. Mater. Interfaces 2014, 6, 9608−9613

indicator of the feasibility of our material for commercialization. The rate capabilities of the C-coated Si/SiO_x electrodes would also be another attractive feature for practical use (Figure 4c). Even at a current density of 2 C (2 A g^{-1}), the electrode maintained more than 90% of its discharge capacity (825.3 mA h g^{-1}) at a rate of 0.05 C (50 mA g^{-1}). This good rate capability of the C-coated Si/SiO_x electrode can be ascribed to the nanoarchitecture of the Si/SiO_x composites, which results in a large interfacial area between the electrolyte and electrode materials and a short diffusion length for Li^+.

Since electrode expansion and cell deformation are the key factors which limit the adoption of Si-based electrodes in commercial LIBs, the dimensional stability and the degree of expansion of the electrode should be minimized. It should be noted that the cycled electrode (right in Figure 4d) did not show any noticeable disintegration, such as cracks and detachment of the electrode from the substrate, compared with the pristine electrode (left in Figure 4d). Moreover, the C-coated Si/SiO_x nanospheres retained their initial morphology without significant degradation after cycling. The electrode showed expansion of the height by about 20.8% after 2 cycles and only 37.5% after 100 cycles (Figures S5 and S6, Supporting Information). This value for the C-coated Si/SiO_x electrode is much lower than that reported for the Si/graphite composite[32] and slightly lower than that for a Si nanotube electrode (54%) after the second cycle[11] and for an urchinlike Si/SiO_x composite (50%) after 70 cycles.[19] The excellent dimensional and mechanical stability of the C-coated Si/SiO_x nanospheres comes from their microstructure, consisting of (i) an amorphous SiO_x matrix that can accommodate the mechanical strains induced by the volume changes in the Si during cycling, (ii) Si/SiO_x particles ~200 nm in size, a size which is helpful in reducing the absolute volume changes of the electrode, and (iii) the free voids between the Si/SiO_x nanospheres created during heat treatment, which may act as a buffer to accommodate the mechanical strains arising from the volume changes. We firmly believe that optimization of the particle size and morphology of the Si/SiO_x nanospheres can further reduce the volume expansion during cycling.

CONCLUSIONS

We have developed a scalable technique to synthesize nanostructured Si/SiO_x nanospheres based on a sol–gel reaction and demonstrated their promising electrochemical performance as a high-capacity lithium storage material. By confining crystalline Si in the amorphous SiO_x matrix on the nanoscale, the severe volume changes of Si can be effectively accommodated. The nanosphere form of the Si/SiO_x composite enables facile electrochemical kinetics by offering a large surface area and short Li^+ pathways. A uniform C coating on the Si/SiO_x nanospheres is also effective for ensuring sufficient electrical conduction, leading to excellent rate capability. We strongly believe that the nontoxic and precious-metal-free approach proposed here will not only expand the design possibilities of Si/SiO_x nanocomposites, but also significantly reduce the production costs of Si/SiO_x nanocomposite anode materials for LIBs.

ASSOCIATED CONTENT

Supporting Information

Figures showing Brunauer–Emmett–Teller (BET) and Barrett–Joyner–Halenda (BJH) data, XRD patterns, SEM images, and TGA curves. This material is available free of charge via the Internet at http://pubs.acs.org.

AUTHOR INFORMATION

Corresponding Authors

*E-mail: yjkim@keti.re.kr.
*E-mail: khansu@hanyang.ac.kr.

Author Contributions

[‖]M.-S.P. and E.P. contributed equally to this work.

Notes

The authors declare no competing financial interest.

ACKNOWLEDGMENTS

This research was supported in part by the Basic Science Research Program through the National Research Foundation of Korea (NRF) funded by the Ministry of Education (Grant. NRF-2012R1A1A2044422), by the research fund of Hanyang University (Grant HY-2012-T), and by the Energy Efficiency & Resources Core Technology Program of the Korea Institute of Energy Technology Evaluation and Planning (KETEP) funded by the Ministry of Trade, Industry & Energy, Republic of Korea (Grant 20132020000260). We thank Dr. H. Y. Jung (Ulsan National Institute of Science and Technology (UNIST), Republic of Korea) for his helpful discussions.

REFERENCES

(1) Jeong, G.; Kim, Y. U.; Kim, H.; Kim, Y. J.; Sohn, H. J. Prospective Materials and Applications for Li Secondary Batteries. *Energy Environ. Sci.* **2011**, *4*, 1986–2002.
(2) Choi, N.; Chen, Z.; Freunberger, S. A.; Ji, X.; Sun, Y.-K.; Amine, K.; Yushin, G.; Nazar, L.; Cho, J.; Bruce, P. G. Challenges Facing Lithium Batteries and Electrical Double-Layer Capacitors. *Angew. Chem., Int. Ed.* **2012**, *51*, 9994–10024.
(3) Cheng, F.; Liang, J.; Tao, Z.; Chen, J. Functional Materials for Rechargeable Batteries. *Adv. Mater.* **2011**, *23*, 1695–1715.
(4) Park, C.-M.; Kim, J.-H.; Kim, H.; Sohn, H.-J. Li-Alloy Based Anode Materials for Li Secondary Batteries. *Chem. Soc. Rev.* **2010**, *39*, 3115–3141.
(5) Wang, J. W.; He, Y.; Fan, F.; Liu, X. H.; Xia, S.; Liu, Y.; Harris, T.; Li, H.; Huang, J. Y.; Mao, S. X.; Zhu, T. Two-Phase Electrochemical Lithiation in Amorphous Silicon. *Nano Lett.* **2013**, *13*, 709–715.
(6) Obrovac, M. N.; Christensen, L.; Le, D. B.; Dahn, J. R. Alloy Design for Lithium-Ion Battery Anodes. *J. Electrochem. Soc.* **2007**, *154*, A849–A855.
(7) Wu, H.; Cui, Y. Designing Nanostructured Si Anodes for High Energy Lithium Ion Batteries. *Nano Today* **2012**, *7*, 414–429.
(8) Szczech, J. R.; Jin, S. Nanostructured Silicon for High Capacity Lithium Battery Anodes. *Energy Environ. Sci.* **2011**, *4*, 56–72.
(9) Beaulieu, B. L. Y.; Hatchard, H. D.; Bonakdarpour, A.; Fleischauer, M. D.; Dahn, J. R. Reaction of Li with Alloy Thin Films Studied by *in Situ* AFM. *J. Electrochem. Soc.* **2003**, *150*, A1457–A1464.
(10) Chan, C. K.; Peng, H.; Liu, G.; McIlwrath, K.; Zhang, F. X.; Huggins, R. A.; Cui, Y. High-Performance Lithium Battery Anodes Using Silicon Nanowires. *Nat. Nanotechnol.* **2008**, *3*, 31–35.
(11) Song, T.; Xia, J.; Lee, J.-H.; Lee, D. H.; Kwon, M.-S.; Choi, J.-M.; Wu, J.; Doo, S. K.; Chang, H.; Park, W. I.; Zang, D. S.; Kim, H.; Huang, Y.; Hwang, K.-C.; Rogers, J. A.; Paik, U. Arrays of Sealed Silicon Nanotubes as Anodes for Lithium Ion Batteries. *Nano Lett.* **2010**, *10*, 1710–1716.
(12) Wu, H.; Chan, G.; Choi, J. W.; Ryu, I.; Yao, Y.; McDowell, M. T.; Lee, S. W.; Jackson, A.; Yang, Y.; Hu, L.; Cui, Y. Stable Cycling of Double-Walled Silicon Nanotube Battery Anodes through Solid–electrolyte Interphase Control. *Nat. Nanotechnol.* **2012**, *7*, 310–315.
(13) Jung, H.; Kim, Y.-U.; Sung, M.-S.; Hwa, Y.; Jeong, G.; Kim, G.-B.; Sohn, H.-J. Nanosize Si Anode Embedded in Super-Elastic Nitinol

(Ni−Ti) Shape Memory Alloy Matrix for Li Rechargeable Batteries. *J. Mater. Chem.* **2011**, *21*, 11213−11216.
(14) Mao, O.; Dahn, J. R. Mechanically Alloyed Sn-Fe(-C) Powders as Anode Materials for Li-Ion Batteries: III. Sn_2Fe:$SnFe_3C$ Active/Inactive Composites. *J. Electrochem. Soc.* **1999**, *146*, 423−427.
(15) Gowda, S. R.; Pushparaj, V.; Herle, S.; Girishkumar, G.; Gordon, J. G.; Gullapalli, H.; Zhan, X.; Ajayan, P. M.; Reddy, A. L. M. Three-Dimensionally Engineered Porous Silicon Electrodes for Li Ion Batteries. *Nano Lett.* **2012**, *12*, 6060−6065.
(16) Lee, J.-I.; Choi, N.-S.; Park, S. Highly Stable Si-Based Multicomponent Anodes for Practical Use in Lithium-Ion Batteries. *Energy Environ. Sci.* **2012**, *5*, 7878−7882.
(17) Jeong, G.; Kim, Y. U.; Krachkovskiy, S. A.; Lee, C. K. A Nanostructured $SiAl_{0.2}O$ Anode Material for Lithium Batteries. *Chem. Mater.* **2010**, *22*, 5570−5579.
(18) Lee, J.-I.; Lee, K.-T.; Cho, J.; Kim, J.; Choi, N.-S.; Park, S. Chemical-Assisted Thermal Disproportionation of Porous Silicon Monoxide into Silicon-Based Multicomponent Systems. *Angew. Chem., Int. Ed.* **2012**, *124*, 2821−2825.
(19) Yoo, H.; Lee, J.-I.; Kim, H.; Lee, J. P.; Cho, J.; Park, S. Helical Silicon/Silicon Oxide Core−Shell Anodes Grown onto the Surface of Bulk Silicon. *Nano Lett.* **2011**, *11*, 4324−4328.
(20) Takezawa, H.; Iwamoto, K.; Ito, S.; Yoshizawa, H. Electrochemical Behaviors of Nonstoichiometric Silicon Suboxides (SiO_x) Film Prepared by Reactive Evaporation for Lithium Rechargeable Batteries. *J. Power Sources* **2013**, *244*, 149−157.
(21) Yamada, M.; Ueda, A.; Matsumoto, K.; Ohzuku, T. Silicon-Based Negative Electrode for High-Capacity Lithium-Ion Batteries: "SiO"-Carbon Composite. *J. Electrochem. Soc.* **2011**, *158*, A417−A421.
(22) Pauthe, M.; Bernstein, E.; Dumas, J.; Saviot, J.; Pradel, A.; Ribes, M. Preparation and Characterisation of Si Nanocrystallites Embedded in a Silica Matrix. *J. Mater. Chem.* **1999**, *9*, 187−191.
(23) Hessel, C. M.; Henderson, E. J.; Veinot, J. G. C. Hydrogen Silsesquioxane: A Molecular Precursor for Nanocrystalline Si−SiO_2 Composites and Freestanding Hydride-Surface-Terminated Silicon Nanoparticles. *Chem. Mater.* **2006**, *18*, 6139−6146.
(24) Kelly, J. A.; Henderson, E. J.; Veinot, J. G. C. Sol−Gel Precursors for Group 14 Nanocrystals. *Chem. Commun.* **2010**, *46*, 8704−8718.
(25) Puzzo, D. P.; Henderson, E. J.; Helander, M. G.; Wang, Z.; Ozin, G. A.; Lu, Z. Visible Colloidal Nanocrystal Silicon Light-Emitting Diode. *Nano Lett.* **2011**, *11*, 1585−1590.
(26) Janotta, A.; Dikce, Y.; Schmidt, M.; Eisele, C.; Stutzmann, M.; Luysberg, M.; Houben, L. Light-Induced Modification of a-SiO_x II: Laser Crystallization. *J. Appl. Phys. (Melville, NY, U.S.)* **2004**, *95*, 4060−4068.
(27) Xie, Z.; Henderson, E. J.; Dag, Ö.; Wang, W.; Lofgreen, J. E.; Kübel, C.; Scherer, T.; Brodersen, P. M.; Gu, Z.-Z.; Ozin, G. A. Periodic Mesoporous Hydridosilica—Synthesis of an "Impossible" Material and Its Thermal Transformation into Brightly Photoluminescent Periodic Mesoporous Nanocrystal Silicon-Silica Composite. *J. Am. Chem. Soc.* **2011**, *133*, 5094−5102.
(28) Miyazaki, H.; Goto, T. SiO_x Films Prepared Using RF Magnetron Sputtering with a SiO Target. *J. Non-Cryst. Solids* **2006**, *352*, 329−333.
(29) Hohl, A.; Wieder, T.; van Aken, P. A.; Weirich, T. E.; Denninger, G.; Vidal, M.; Oswald, S.; Deneke, C.; Mayer, J.; Fuess, H. An Interface Clusters Mixture Model for the Structure of Amorphous Silicon Monoxide (SiO). *J. Non-Cryst. Solids* **2003**, *320*, 255−280.
(30) Miyachi, M.; Yamamoto, H.; Kawai, H.; Ohta, T.; Shirakata, M. Analysis of SiO Anodes for Lithium-Ion Batteries. *J. Electrochem. Soc.* **2005**, *152*, A2089−A2091.
(31) Ogata, K.; Salager, E.; Kerr, C. J.; Fraser, A. E.; Ducati, C.; Morris, A. J.; Hofmann, S.; Grey, C. P. Revealing Lithium−Silicide Phase Transformations in Nano-Structured Silicon-Based Lithium Ion Batteries via *in Situ* NMR Spectroscopy. *Nat. Commun.* **2014**, *5*, 3217.
(32) Hwang, S. S.; Cho, C. G.; Kim, H. Polymer Microsphere Embedded Si/Graphite Composite Anode Material for Lithium Rechargeable Battery. *Electrochim. Acta* **2010**, *55*, 3236−3239.